Simulation of Wave-Plus-Current Scour beneath Submarine Pipelines

Larsen, Bjarke Eltard; Fuhrman, David R.; Sumer, B. Mutlu

Published in:
Journal of Waterway, Port, Coastal, and Ocean Engineering

Link to article, DOI:
10.1061/(ASCE)WW.1943-5460.0000338

Publication date:
2016

Document Version
Peer reviewed version

Simulation of wave-plus-current scour beneath submarine pipelines

Bjarke Eltard Larsen[1] [2], David R. Fuhrman [3], B. Mutlu Sumer [4]

ABSTRACT

A fully-coupled hydrodynamic and morphologic numerical model is utilized for the simulation of wave-plus-current scour beneath submarine pipelines. The model is based on incompressible Reynolds-averaged Navier-Stokes equations, coupled with k-ω turbulence closure, with additional bed and suspended load descriptions forming the basis for seabed morphology. The model is successfully validated against experimental measurements involving scour development and eventual equilibrium in pure-current flows, over a range of Shields parameters characteristic of both clear-water and live-bed regimes. This validation complements previously demonstrated accuracy for the same model in simulating pipeline scour processes in pure-wave environments. The model is subsequently utilized to simulate combined wave-plus-current scour over a wide range of combined Keulegan-Carpenter numbers and relative current strengths. The resulting equilibrium scour depths and trends are shown to be in accordance with existing experimentally-based expressions from the literature. The variety of scour profile types emerging under various flow conditions is detailed, and reconciled with experimental observations. The resulting matrix of scour depth time series are systematically analysed, resulting in a new generalized expression for the scour time scale in combined wave-plus-current flow environments. This expression is fully-consistent with existing experimentally-based relations at both pure-current and pure-wave limits, and is

[1]Ph.D. Student, M.Sc. Technical University of Denmark, Department of Mechanical Engineering, Section of Fluid Mechanics, Coastal and Maritime Engineering, DK-2800 Kgs. Lyngby, Denmark

[2]Corresponding author, bjelt@mek.dtu.dk

[3]Associate Professor. Technical University of Denmark, Department of Mechanical Engineering, Section of Fluid Mechanics, Coastal and Maritime Engineering, DK-2800 Kgs. Lyngby, Denmark

[4]Professor Emeritus. Technical University of Denmark, Department of Mechanical Engineering, Section of Fluid Mechanics, Coastal and Maritime Engineering, DK-2800 Kgs. Lyngby, Denmark

appropriate for engineering use.

Keywords: Scour, Pipelines, Sediment transport, Morphology, Combined waves and current, Time scale, Turbulence modelling, k-ω model

INTRODUCTION

Scour beneath submarine pipelines has been the subject of much past research (see *e.g.* Hoffmans and Verheij, 1997; Whitehouse, 1998; Sumer and Fredsøe, 2002, for a general introduction). Most research has been in the form of laboratory experiments, though in more recent years a large number of numerical investigations have emerged as computational power has increased. The earliest attempts to model scour beneath pipelines were made using potential flow models, whereas more recent attempts were carried out by solving the complete Navier-Stokes equations, either in the form of the Reynolds-averaged Navier-Stokes equations (RANS), or using Large Eddy Simulation (LES). Brørs (1999), Liang and Cheng (2005b), Liang et al. (2005) Zhao and Fernando (2007), and Zanganeh et al. (2012) succeeded in modelling the scour evolution beneath pipelines in steady currents and Liang and Cheng (2005a), Kazeminezhad et al. (2012) and Fuhrman et al. (2014) modelled the scour beneath a pipeline due to waves. Fuhrman et al. (2014) demonstrated accurate scour time scales, while also managing to simulate the backfilling process caused by a change to milder wave conditions.

To date most research, both numerical and experimental, has focussed on scour induced by either pure waves or currents, while comparatively few studies have involved combined wave-plus-current environments. Of these, Lucassen (1984) carried out a series of experiments for a rather limited set of waves and currents, while Sumer and Fredsøe (1996) carried out scour depth investigations for a comprehensive range of combined waves and currents. The experimental studies focused primarily on the equilibrium scour depth, thus little is known regarding the time scale of scour in generalized wave-plus-current cases. More recently, Myrhaug et al. (2009) focused on scour depth below pipelines due to second-order random waves plus currents and Cheng et al. (2014) investigated the scour propagation speed

along the length of the pipeline. Numerically wave-plus-current scour beneath pipelines has only been investigated using potential flow models, e.g. Bernetti et al. (1990) and Hansen (1992).

The present study focuses on the numerical simulation of wave-plus-current induced scour beneath submarine pipelines, based on a model solving Reynolds-averaged Navier-Stokes (RANS) equations, fully coupled with turbulence closure, bed and suspended load sediment transport descriptions, and a seabed morphological model. The motivation is three-fold: As wave-plus-current scour has yet to be simulated in a fully-coupled numerical model, the first goal is to establish detailed model accuracy in accordance with the steady flow experiments of Mao (1986), as well as for equilibrium scour depths in accordance with the wave-plus-current experiments of Sumer and Fredsøe (1996). The second goal is to investigate the scour process in detail, shedding light on the variety of equilibrium scour profiles that may emerge under various flow conditions. Thirdly, we wish to quantify the pipeline scour time scale for generalized wave-plus-current environments. The goal is to formulate an analytical physically-based expression for this quantity that is fully consistent with existing expressions at both pure-wave and pure-current limits.

MODEL DESCRIPTION

In this section the utilized model is briefly described. As the model has already been described in detail by Fuhrman et al. (2014) the reader is referred to this work for further details. The flow is simulated by solving the incompressible Reynolds-averaged Navier-Stokes equations (RANS) and the continuity equation, coupled with the two-equation k-ω turbulence model by Wilcox (2006, 2008) for closure.

Model boundary conditions are as follows: Friction wall boundaries, i.e. the pipeline and the seabed, utilize a no-slip condition such that velocities are zero. The top boundary is modelled as a frictionless lid meaning that vertical velocities are set to zero, and horizontal velocities and scalar hydrodynamic quantities have zero gradient. This means that the top boundary does not represent the free surface of real waves. At the bottom boundary a

hydraulically rough wall will be assumed, with the friction velocity U_f determined from the tangential velocity at the nearest cell center based on an assumed logarithmic velocity distribution. The friction velocity is then used to calculate k and ω in the cell nearest to the wall with standard wall functions as described by Fuhrman et al. (2014). The pipeline surface will be modelled as a hydraulically smooth wall, utilizing a generalized wall function approach based on the profile of Cebeci and Chang (1978) as also detailed by Fuhrman et al. (2014).

The flow is driven by a Dirichlet condition i.e. a specified velocity at the left-hand inlet boundary, which comes from a separate one-dimensional vertical (1DV) pure boundary layer simulation, made utilizing the same model as described above. In this boundary layer simulation the flow is driven by a body force given by:

$$F = U_m \frac{2\pi}{T_w} \cos\left(\frac{2\pi}{T_w} t\right) + \frac{U_{fc}^2}{h} \tag{1}$$

where U_m is the maximum free stream velocity of the oscillating flow, T_w is the wave period, U_{fc} is the desired friction velocity of the current alone, t is time, and h is the domain height. The simulation is continued until a periodic repetitive state is reached. From here the velocity profile, as well as the profiles for k and ω, are sampled over a single period which are then repeated periodically as inlet boundary conditions within the scour simulations. Through this approach the special characteristics of the combined wave-current boundary layer are incorporated directly within the driving inlet flow, e.g. the well-known apparent roughness effect of a turbulent wave boundary layer on the current (see e.g. Fredsøe et al. (1999)). At the same time the computational time required is kept low, since the long time required (hundreds to thousands of periods) to achieve a fully-developed wave-plus-current flow is simulated entirely within the 1DV framework.

The model for the bed load transport corresponds to that of Roulund et al. (2005), who extended the model of Engelund and Fredsøe (1976) to also include three dimensional

effects as well as bed slope modifications to the Shields parameter. The suspended load is calculated by solving the advection-diffusion equation for the concentration (see *e.g.* Fredsøe and Deigaard, 1992, p. 238). The equation for the suspended sediment is solved on a sub-set of the main computational mesh where the near-bed cells below a given reference level b are removed. At this reference level a reference concentration, c_b, boundary condition is imposed. There are several formulations of c_b but here the one by Engelund and Fredsøe (1976) is utilized.

The morphological updating routine is based on the sediment continuity (Exner) equation as described by Jacobsen et al. (2014). The Exner equation is based on instantaneous sediment transport fields and, therefore, the morphological and hydrodynamic times are equivalent. To ensure that the bed slopes do not exceed the angle of repose the sand slide model described in detail by Roulund et al. (2005) is implemented. In the present work, this model is activated at positions where the local bed angle exceeds the angle of repose $\phi_s = 32°$, and is de-activated once the local bed angle has been reduced to 31.9°.

The equations comprising the fully-coupled model outlined above are solved numerically using the open-source computational fluid dynamics (CFD) toolbox OpenFOAM®, version 1.6-ext, making use of a finite volume spatial discretization with a collocated variable arrangement, in conjunction with a standard pressure-implicit with splitting of operators (PISO) algorithm. For further details see Jacobsen et al. (2014). As noted previously, the fully-coupled model presented above has also been utilized recently by Fuhrman et al. (2014) in the simulation of wave-induced scour beneath submarine pipelines, as well as by Baykal et al. (2015) who simulated the current-induced scour process around a vertical monopile cylinder. The hydrodynamic model can likewise be considered a single-phase variant of the two-phase (air-water) model presented in Jacobsen et al. (2012).

MODEL SET-UP

For all forthcoming simulations the height of the domain has been set to $h = 10D$, where D is the pipeline diameter. The horizontal span has, in most cases, been set to

$-20D \leq x \leq 20D$, but has gradually been changed to $-15D \leq x \leq 40D$ for cases involving strong mean currents, as this promotes more asymmetric scour profiles. The pipeline is placed on the bed with its bottom at the origin $(x, y) = (0, 0)$. For numerical reasons an initial scour hole is needed to provide space for computational cells beneath the pipeline. The initial hole is sinusoidal with a depth of $S_0/D = 0.15$. The computational mesh is graded, such that near the pipeline the smallest cells have height equal to $0.003D$, whereas at the seabed cells are set to have a height $0.5d$, d being the grain size diameter. Between the pipeline and the bed different mesh gradings have been used. Experience has shown that rapidly deepening scour holes can distort the mesh, and to combat this it has been necessary to increase the mesh resolution in certain cases where this proved problematic. This has resulted in computational domains having a cell count between 8732–18,134. In Figure 1 a typical mesh in the near vicinity of the pipeline is shown as an example.

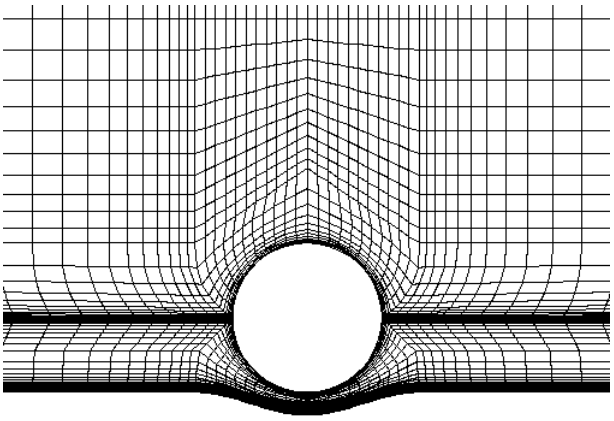

FIG. 1. Example of the computational mesh used for the scour cases.

VALIDATION

In this section the numerical model described above will be validated for scour depth and profile development beneath pipelines subject to steady current flow. For further validation of the present model see the recent work of Fuhrman et al. (2014), who accurately simulated pure wave-induced scour and backfilling processes utilizing the same model. The model results will here be compared with those presented in Mao (1986). Mao (1986) tested

current-induced scour development in both clear-water and live-bed regimes. These experiments provide an excellent benchmark, as scour profiles are available throughout the development, enabling detailed comparison of the simulated and experimental scour processes and development.

Mao (1986) presents results for current-induced scour with pipeline diameter $D = 0.1$ m and sediment grain size $d = 0.36$ mm, for cases yielding far-field Shields parameter

$$\theta = \frac{\tau_b}{\rho g(s-1)d} = \frac{U_f^2}{(s-1)gd} = 0.048 \tag{2}$$

for the clear water case, and $\theta = 0.098$ for the live bed case. Here τ_b is the bed shear stress, g is the gravitational acceleration and $s = 2.65$ is the relative sediment density. For the purposes of the present validation, we aim to effectively maintain Shields parameter similarity with the cases of Mao (1986), while utilizing (hence directly validating) the same computational mesh as in the forthcoming wave-plus-current scour simulations i.e. with $D = 0.03$ m and $d = 0.19$ mm. We will thus compare with the experimental results from Mao (1986) in terms of length scales (hence scour depth) normalized by the pipeline diameter, and in terms of dimensionless morphological time defined by

$$t^* = \frac{\sqrt{g(s-1)d^3}}{D^2}t, \tag{3}$$

which accounts for the cross-sectional area of the scour hole scaling as D^2. Here t is the physical time. Such comparison is justified in a non-dimensional sense, since the expected equilibrium scour depth-to-pipeline diameter ratio is well-known to be approximately constant (Sumer and Fredsøe, 1990)

$$\frac{S_c}{D} = 0.6 \pm 0.2 \tag{4}$$

whereas the dimensionless time scale of the scour development depends only on θ (Fredsøe et al., 1992). Note that for physical consistency, in the simulation of the clear-water case we

have reduced the Shields parameter slightly to $\theta = 0.044$, to ensure that the far-field Shields parameter is indeed below the critical value $\theta_c = 0.045$ assumed in the model formulation.

The steady current flows are driven from the inlet as described previously, based on results from a prior 1DV simulation driven by the body force (1) with $U_m = 0$ (i.e. no waves) and with friction velocity U_{fc} chosen to yield the desired θ according to (2). Since an initial scour hole is specified in the model, whereas the experiments by Mao (1986) started from a plane bed, it is necessary to compensate for the approximate time required to achieve the initial scour depth. This has been achieved by evaluating the initial simulated rate of scour dS/dt and extrapolating back in time to $S = 0$, leading to a shifted time given by $t'^* = t^* + t^*_{shift}$. For the validation cases a warm up period of $t = 30$ s is utilized, during which the morphology is switched off, and the hydrodynamic and sediment transport fields are allowed to become fully developed. At the end of this warm up period the morphology is switched on, with this time denoted as $t = 0$.

In Figure 2 the time series of the non-dimensional scour depth, taken as the vertical clearance beneath the center of the pipeline, is shown as a function of non-dimensional time for both the clear-water (Figure 2a) and the live-bed (Figure 2b) regimes. Also included in the figure are the temporal scour depth measurements from the experiments of Mao (1986). It can be seen that in both cases most of the scour occurs relative quickly, followed by a slow increase in the scour depth until equilibrium is reached. From this figure it is seen that the model predicts similar scour evolution, as well as equilibrium scour depths, as in the experiments. In both clear-water and live-bed regimes the predicted equilibrium scour is slightly below that observed experimentally. As further validation, the computed and measured (Mao, 1986) scour profiles at various non-dimensional times are compared in Figure 3, for both the clear-water (left) and live-bed (right) cases. Again, in both cases, it can be seen that most of the scour occurs rapidly, as the scour is already appreciable in the earliest snapshots. Alternatively, the increase in scour width and the migration of the downstream shoulder requires substantially longer time. The first phase of the observed

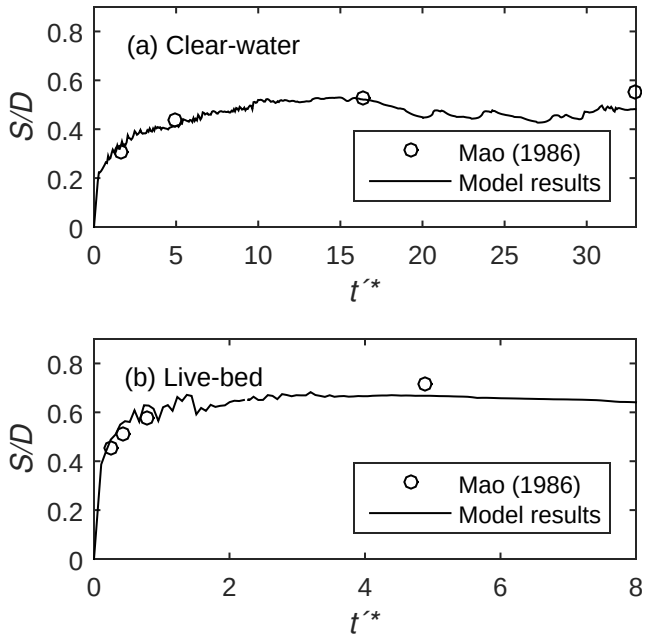

FIG. 2. Comparison of modelled and experimental non-dimensional scour depth. Experimental data taken from Mao (1986). (a) Clear-water, with $\theta = 0.048$ and $D = 0.1$ m in the experiments, and $\theta = 0.044$ and $D = 0.03$ m in the model results.(b) Live-bed, with $\theta = 0.098$ and $D = 0.1$ m in the experiments, and $\theta = 0.098$ and $D = 0.03$ m in the model results.

scour corresponds to tunnel erosion, where a large amount of water is forced through the small gap between the pipeline and the bed, resulting in large amplification of the bed shear stress and thus a rapid increase in the scour depth. The second corresponds to the lee-wake erosion phase, where vortices convect sediment downstream. The model results compare quite well with the experimental results from Mao (1986) throughout both phases, as seen by the consistently good profile match in Figure 3. Hence, this comparison demonstrates the ability of the model to capture not only the scour depth evolution, but also the bed profile morphology in both the clear-water and the live-bed cases. Note that in the live-bed case a small difference can, however, be seen at $t^{'*} = 4.95$, Figure 3f. This can be attributed to the formation of bedforms developing upstream of the pipeline, which shield the flow. While deviating slightly from the observed profile in this detail, it is emphasized that the development of such bedforms is, in fact, an expected physical phenomenon in the live-bed regime. We regard the resemblance in the computed results and the experiments by Mao

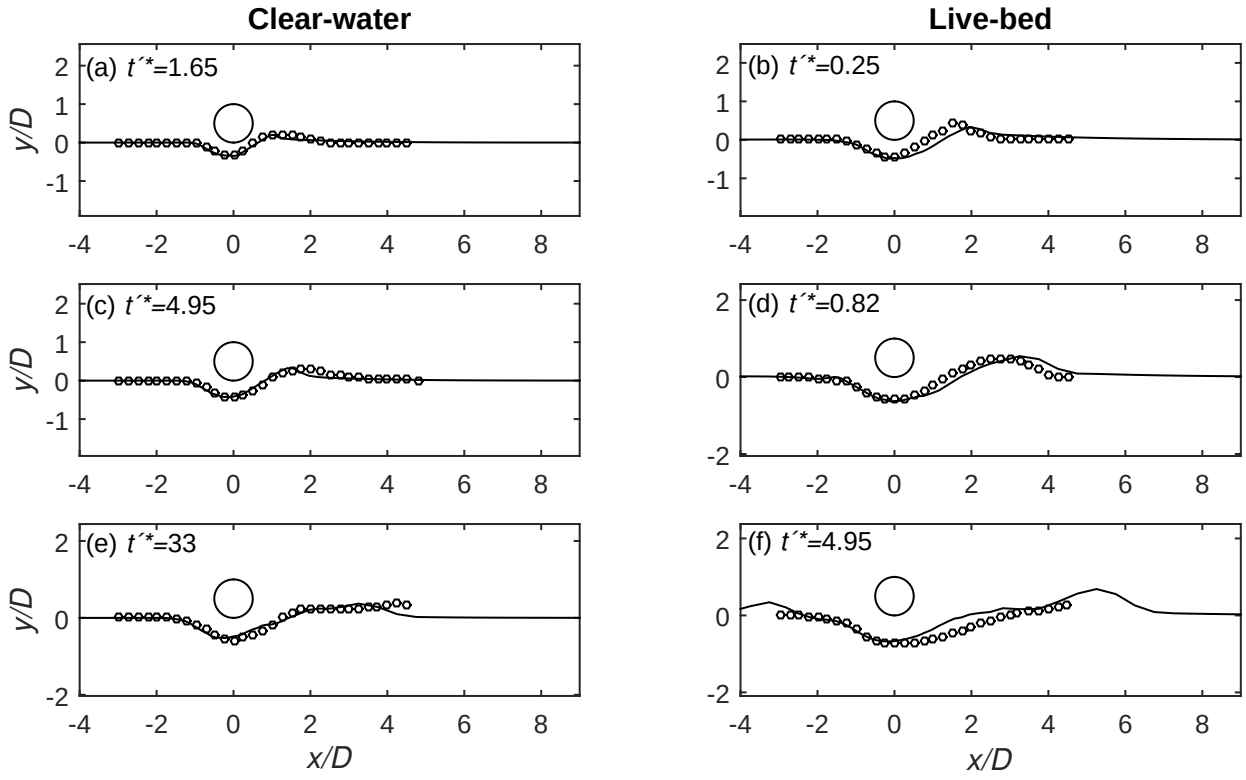

FIG. 3. Comparison of modelled (cirles) and experimental (lines) scour profiles at different times. Experimental data taken from Mao (1986). Left, clear-water, with $\theta = 0.048$ and $D = 0.1$ m in the experiments, and $\theta = 0.044$ and $D = 0.03$ m in the model results. Right, live-bed, with $\theta = 0.098$ and $D = 0.1$ m in the experiments, and $\theta = 0.098$ and $D = 0.03$ m in the model results.

(1986) as still acceptable, even at this later stage in the profile development.

As a final test of the model accuracy, a number of additional steady-current scour cases have been simulated, to systematically check the Shields parameter-dependence on the equilibrium scour depth with that evident from the experiments of Mao (1986). For this purpose six additional values $\theta = 0.026, 0.055, 0.073, 0.117, 0.143, 0.172$ have been selected, and simulated until equilibrium scour is reached, as before. The resulting equilibrium scour depths for all (eight) cases considered are then plotted as a function of θ in Figure 4, as are the experimental results reported by Mao (1986). From this figure, it is seen that the computed equilibrium scour depth dependence resembles that of Mao (1986) over the full range of θ considered, starting within the clear-water regime and extending well into the live-bed regime. The scour depth in the experiments reaches an equilibrium value of $S/D \approx 0.8$–0.9 at slightly

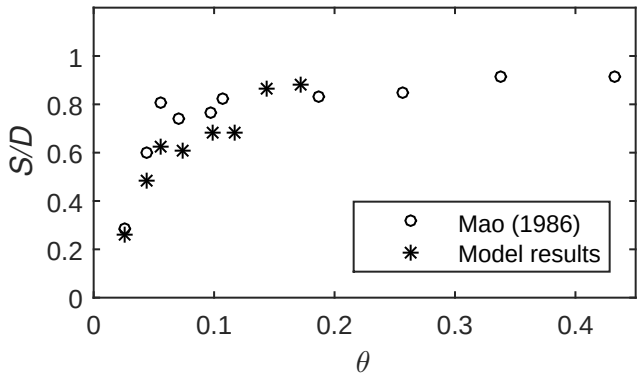

FIG. 4. Equilibrium scour depth versus Shields parameter for both experimental, data taken from Mao (1986), with $\theta \approx 0.03 - 0.43$ and $D = 0.05 - 0.1$ m, and modelled, with $\theta = 0.026$–0.172 and $D = 0.03$ m.

lower θ than predicted by the model. For low values of θ the equilibrium scour depths match the experimentally-based empirical expression (4) quite well, whereas for $\theta > 0.15$ the scour depths are slightly larger, around $S/D \approx 0.9$. This is generally consistent with the results from Mao (1986). As seen, all of the computed and experimental results for the live-bed equilibrium scour are within 1 to 1.5 standard deviations of the mean predicted by (4).

Based on the results presented above, the model has demonstrated the ability to reliably predict current-induced scour processes beneath a submarine pipeline, both in terms of the equilibrium scour depths, as well as the resulting morphological development of the surrounding bed profile. These results are complemented by those presented previously by Fuhrman et al. (2014).

SIMULATION OF WAVE-PLUS-CURRENT SCOUR

Having collectively validated the model for both current-induced scour (above), as well as wave-induced scour (Fuhrman et al., 2014), it will now be utilized for the numerical study of combined wave-plus-current scour processes beneath pipelines. In the following the results of seventy seven new wave-plus-current scour cases will be presented and analysed. The cases considered will consist of waves characterized by ten different Keulegan-Carpenter numbers, KC:

$$KC = \frac{U_m T_w}{D} \tag{5}$$

and up to eight different values of the parameter m:

$$m = \frac{U_c}{U_c + U_m}, \tag{6}$$

which defines the relative strength of the current i.e. $m = 0$ corresponds to pure-wave conditions, with $m = 1$ corresponding to pure-current conditions, where U_c is the current velocity at the center of the pipeline. The discrete values of the current are selected such that $m = 0, 0.1, 0.2, \ldots, 0.7$. The previously considered eight pure-current results will likewise be utilized to characterize $m = 1$. In Table 1 a summary of the new cases can be seen, organized by their respective KC values. The table also provides the range of the far-field Shields parameter, θ_{cw}, which can be interpreted as the maximum Shields parameter of the combined wave-current flow, calculated by utilizing an equivalent to the formula given by Soulsby (1995).

$$\theta_{cw} = \theta_m + \theta_w \tag{7}$$

where

$$\theta_m = \theta_{cur}\left(1 + 1.2\left(\frac{\theta_w}{\theta_{cur} + \theta_w}\right)^{3.2}\right) \tag{8}$$

is the mean Shields parameter. Here θ_{cur} is the Shields parameter coming from the current alone calculated from friction velocity U_{fc} (taken directly from the input of the boundary layer simulations, (1)) and θ_w is the maximum Shields parameter of the oscillating flow, calculated from the maximum friction velocity of the oscillating flow, taken as

$$U_{fw} = \sqrt{0.5 f_w} U_m. \tag{9}$$

For convenience, f_w is taken as the maximum of the laminar, smooth-turbulent, and rough-turbulent wave friction factors i.e. $f_w = \max[f_w^{lam}, f_w^{smooth}, f_w^{rough}]$. For this purpose f_w^{lam} is calculated theoretically as:

$$f_w^{lam} = \frac{2}{\sqrt{Re}}, \tag{10}$$

f_w^{smooth} is calculated from the expression of Fredsøe and Deigaard (1992):

$$f_w^{smooth} = 0.035 Re^{-0.16}, \tag{11}$$

where $Re = U_m a/\nu$ is the Reynolds number, and the empirical expression from Fuhrman et al. (2013)

$$f_w^{rough} = \exp\left(5.5\left(\frac{a}{k_s}\right)^{-0.16} - 6.7\right) \tag{12}$$

is utilized for the rough-wall regime. To check that (7) is representative of the maximum computed Shields parameter it is been plotted as a function the maximum far field Shields parameters taken directly from the model in Figure 5. This figure confirms that (7) is an

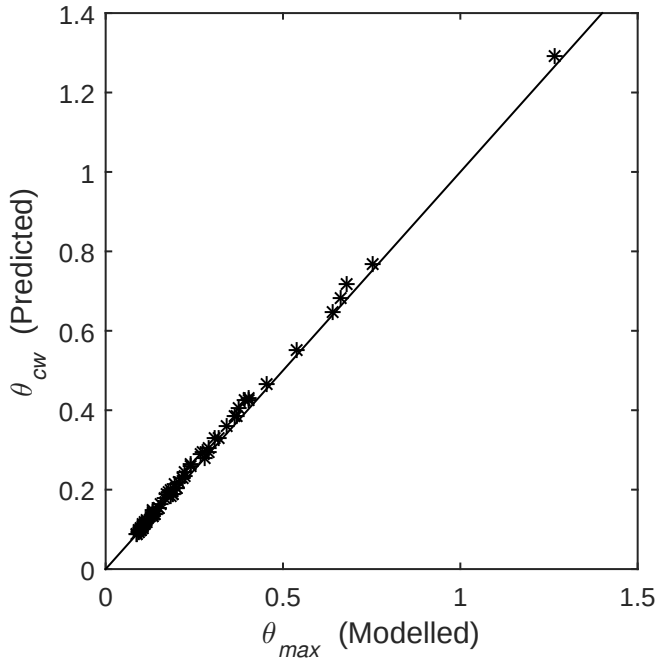

FIG. 5. Fit between maximum computed Shields parameters from the model and the predicted Shields parameters from (7) as proposed by Soulsby (1995).

excellent representation of the maximum far field Shields parameter as a nearly perfect match is achieved

Following the methodology of Fuhrman et al. (2014), for all cases considered, a warm up period of $10T_w$ is used, during which time the morphology is switched off. This is again done

TABLE 1. Summary of cases considered for wave-plus-current induced scour beneath submerged pipelines. All cases use pipeline diameter $D = 0.03$ m and grain diameter $d = 0.19$ mm.

KC	T_w (s)	U_m (m/s)	U_c (m/s)	m	θ_{cw}
5.6	1.10	0.153	0–0.357	0–0.7	0.119–0.327
11	1.22	0.240	0–0.360	0–0.6	0.177–0.432
15	2.50	0.177	0–0.413	0–0.7	0.088–0.386
19.6	3.00	0.196	0–0.457	0–0.7	0.092–0.464
21.1	2.64	0.239	0–0.558	0–0.7	0.120–0.681
25.3	3.51	0.216	0–0.504	0–0.7	0.110–0.550
30	3.50	0.257	0–0.600	0–0.7	0.120–0.768
35	2.70	0.388	0–0.388	0–0.5	0.260–0.431
48	6.00	0.240	0–0.560	0–0.7	0.089–0.649
51	4.50	0.340	0–0.793	0–0.7	0.176–1.290

to allow both the hydrodynamic and sediment transport fields to fully develop. At the end of the warm up period the morphology is switched on, with this time denoted as $t = 0$.

Scour time series

For all cases the scour depth S, again taken directly beneath the pipeline center, has been monitored. The simulations have proceeded until an apparent equilibrium is reached, i.e. when the scour curve has flattened and maintained a fairly constant value over a significant duration. As examples, Figures 6 and 7 show the computed non-dimensional scour depth, S/D as a function of non-dimensional time, t^*, for cases having fixed $KC = 19.6$ and $KC = 30$, for each of the eight m values considered. It can be seen that the scour process begins immediately after the morphology is switched on, with the scour depth increasing until equilibrium is reached, similar to before. The computed equilibria are dynamic, rather than static, as the scour depth is seen to fluctuate slightly even after long-term trends have vanished.

The other KC numbers investigated demonstrate temporal scour developments quite similar to the those shown in Figures 6 and 7. The lone exceptions are cases having $KC = 11$ in combination with low values of m (i.e. weak currents), in which the temporal scour process typically follows two separate phases: The first resembles the usual evolution as

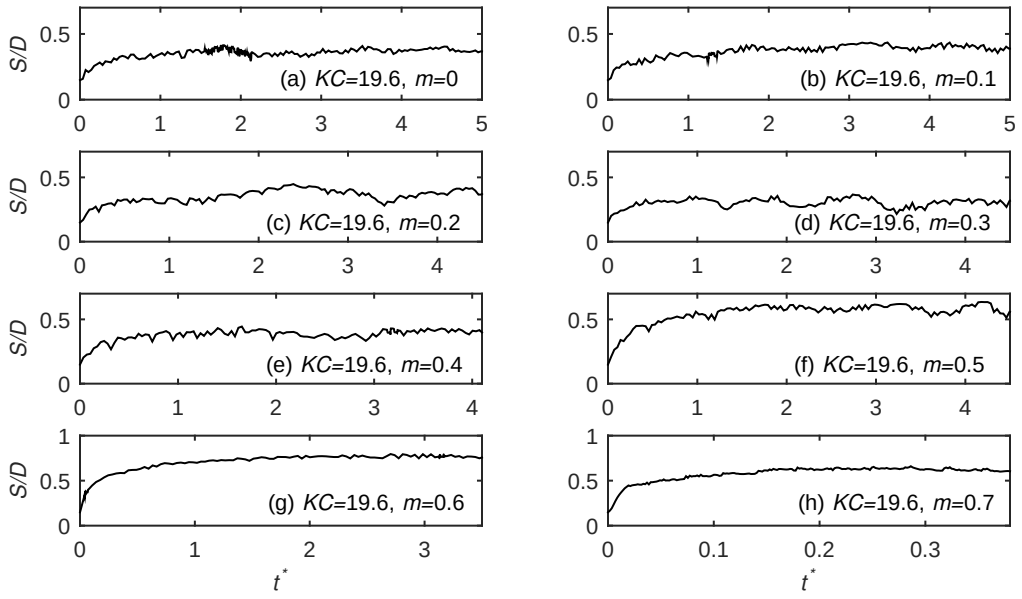

FIG. 6. Simulated scour development for combined wave-plus-current cases having fixed $KC = 19.6$ with different values of m.

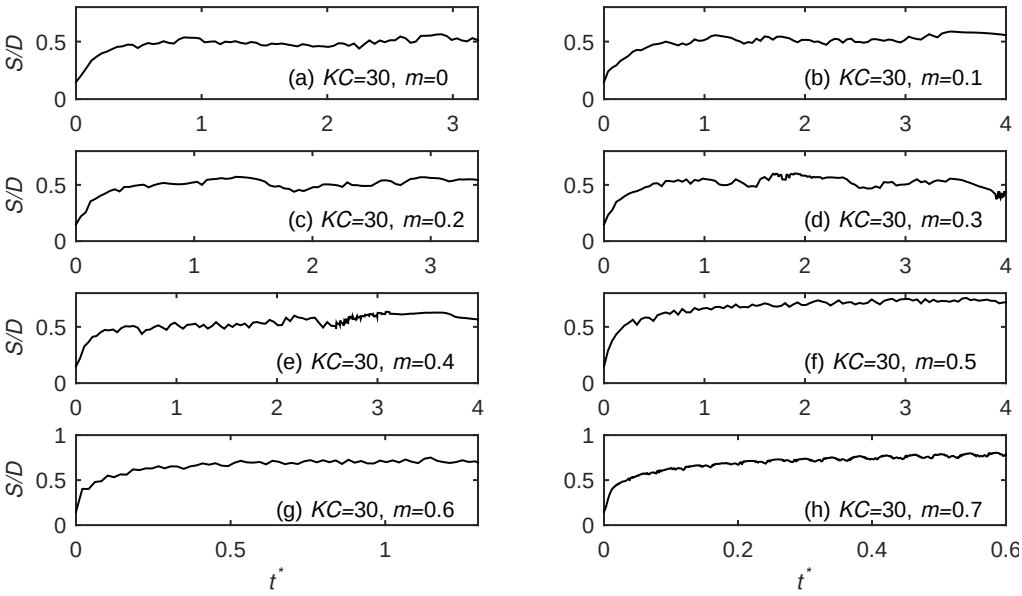

FIG. 7. Simulated scour development for combined wave-plus-current cases having fixed $KC = 30$ with different values of m.

in Figures 6 and 7, which is then followed by a second phase of excessive scour. This behaviour is consistent with that observed and detailed in the previous pure-wave simulations of Fuhrman et al. (2014) for $KC = 11$. They explained the second phase as part of a resonance phenomenon excited within the model, wherein profile wavelengths developing

beneath the pipeline match closely those expected for vortex ripples in this KC range. As this phenomenon has already been explained and illustrated in detail by Fuhrman et al. (2014), for brevity we do not present further details here. Following Fuhrman et al. (2014), however, for the four cases of $KC = 11$ with $m \leq 0.3$ where this behaviour is evident, only the first simulated scour phase is considered in what follows, as this is seemingly consistent with what has been observed experimentally.

Equilibrium scour depth

We will now compare the computed equilibrium scour depths with existing experimentally-based empirical expressions from the literature. The equilibrium scour depths from all of the wave-plus-current model simulations, here taken as the average scour depth over several periods after the equilibrium scour depth has been reached, are now summarized in Figure 8 for the ten different KC numbers combined with up to eight different values of m. Included as the full line in each subplot is also the empirical relation given by Sumer and Fredsøe (1996):

$$S_e = S_c F \tag{13}$$

where S_c is the equilibrium scour depth from the current alone (4), and F is given by

$$F = \begin{cases} \frac{5}{3}\left(KC\right)^{a_m} exp\left(2.3 b_m\right), & 0 \leq m \leq 0.7 \\ 1, & m > 0.7 \end{cases} \tag{14}$$

where a_m and b_m depend on m according to:

$$a_m = \begin{cases} 0.557 - 0.912\left(m - 0.25\right)^2, & 0 \leq m \leq 0.4, \\ -2.14m + 1.46, & 0.4 < m \leq 0.7, \end{cases} \tag{15}$$

$$b_m = \begin{cases} -1.14 + 2.24\,(m - 0.25)^2\,, & 0 \leq m \leq 0.4, \\ 3.3m - 2.5, & 0.4 < m \leq 0.7. \end{cases} \tag{16}$$

The additional dashed lines in Figure 8 denote plus or minus the standard deviation (i.e. $\pm 0.2 S_e/D$) about the mean equilibrium scour from (13), as implied by (4).

Generally, it can be seen that the modelled equilibrium scour depths for combined wave-plus-current flow compare reasonably with the experimentally-based prediction (13) for all the cases considered. This further validates the model for simulated wave-plus-current scour conditions. The general trend of the scour depth in relation to m is as follows: For low values of m the scour depth is quite close to the pure-wave case; as m is increased beyond $m = 0.4$–0.5 the scour depth increases, and for $m \geq 0.5$ the scour depths are effectively very similar to those in pure-current flows. These findings are again consistent with the experimental result of Sumer and Fredsøe (1996). There is, however, a tendency for the modelled equilibrium scour depths to be slightly larger than predicted by (13) i.e. towards the upper limit of the standard deviation, in cases where m is high. This is as expected since $\theta_{cw} > 0.15$ in such cases, hence these results are consistent with the steady-current results shown in Figure 4, where the equilibrium scour depth lies in the range of $0.8 < S_c/D < 0.9$ when $\theta > 0.15$. The same argument explains why the cases with $KC = 35$ also lie close to the upper limit of the standard deviation, since these cases, likewise, all result in high far-field Shields parameters.

Scour profiles

The present section will now detail the various types of equilibrium scour profiles that develop within the combined wave-plus-current scour simulations, as well as describe the range of flow conditions under which each type emerges. The results of the present numerical study have shown that combined current and wave climates can yield a variety of equilibrium profile shapes, depending on the combination of KC and m. In what follows, we identify three different profile classes, which can be characterized as: (1) those resembling profiles seen in steady currents, (2) those resembling profiles seen in pure waves, and (3) those markedly

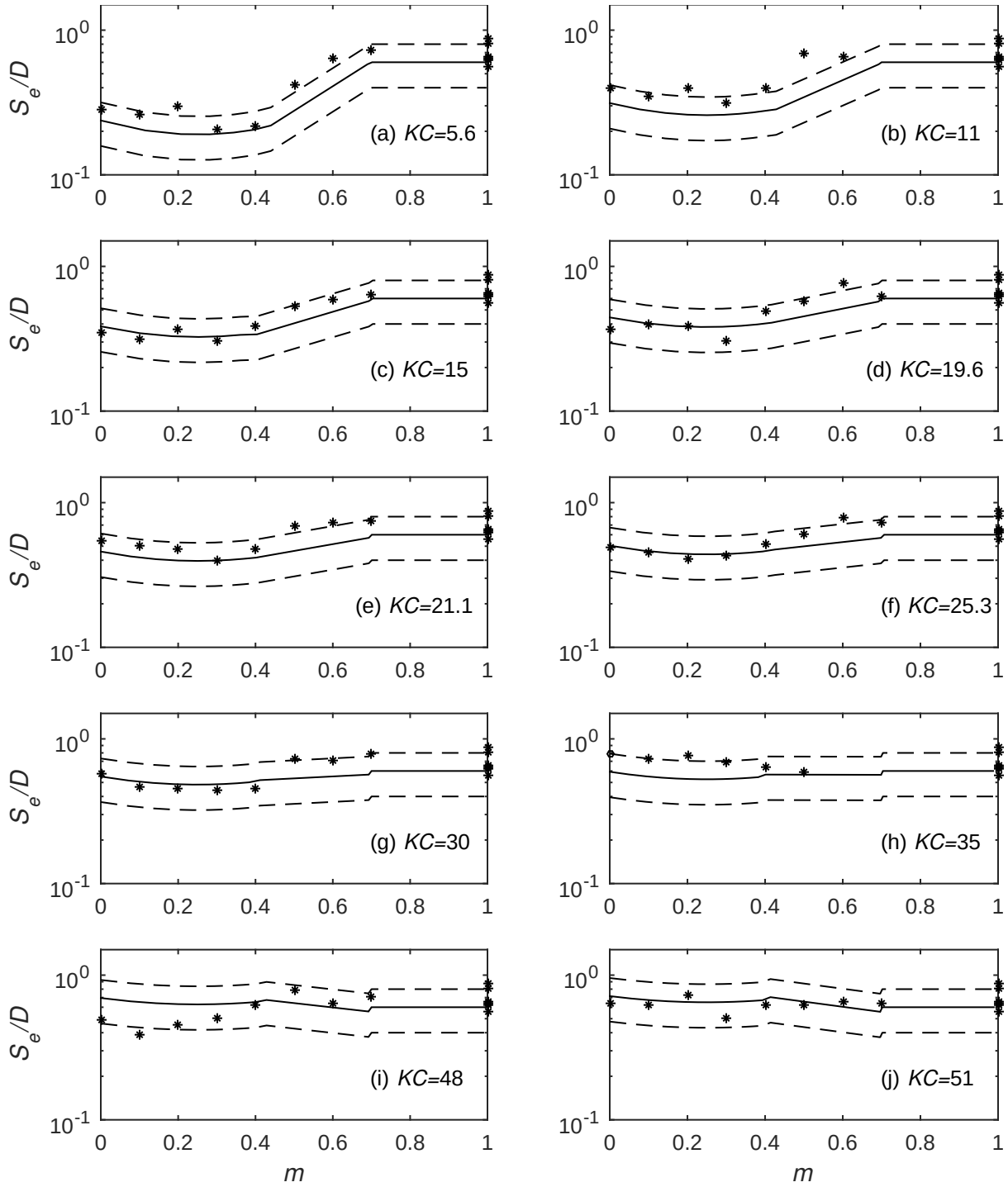

FIG. 8. Equilibrium scour depths. Solid lines: Empirical expression (13) from Sumer and Fredsøe (1996). Asterisk symbols: Results from the present numerical simulations. Dashed lines indicate standard deviation implied by incorporation of (4) in (13).

different than observed in either pure-current or pure-wave climates, to be described in more detail.

Profiles resembling those from steady-current scour emerge in cases where the parameter m is large, typically $m \geq 0.6$, as should be expected, intuitively. Perhaps more surprisingly, such profiles have also been identified in simulations with somewhat lower $m \geq 0.4$, provided that $KC \geq 35$. The development in the latter cases i.e. with moderate m combined with sufficiently large KC, can be attributed to the large stroke of the wave, which induces pronounced erosion beneath the pipeline when the oscillatory flow follows, rather than opposes, the current. Examples of the scour profile developed under both scenarios are depicted in Figure 9. Although KC and m are rather different, the resulting bed profiles for

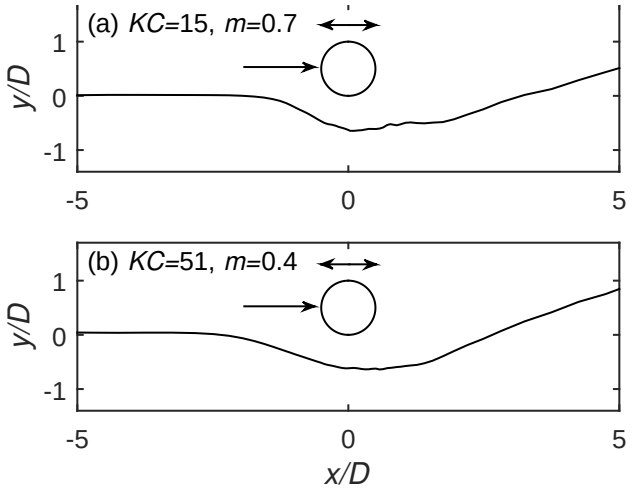

FIG. 9. Equilibrium scour profile of $KC = 15$, $m = 0.7$ and $KC = 51$, $m = 0.4$.

these two cases in the vicinity of the pipeline are both quite similar to those seen previously in pure-current flows, see again Figure 3. Further away from the pipeline some differences emerge, especially downstream of the pipeline. Here the shoulder in the current-dominated case (Figure 9a) is almost completely eroded whereas the shoulder is more pronounced in the case with an intermediate value of m (Figure 9b). In Figure 10 equilibrium profiles from three different cases with low $m = 0.2$ are shown. For such low values of m the resulting equilibrium scour profiles resemble closely those for pure waves as expected. These are char-

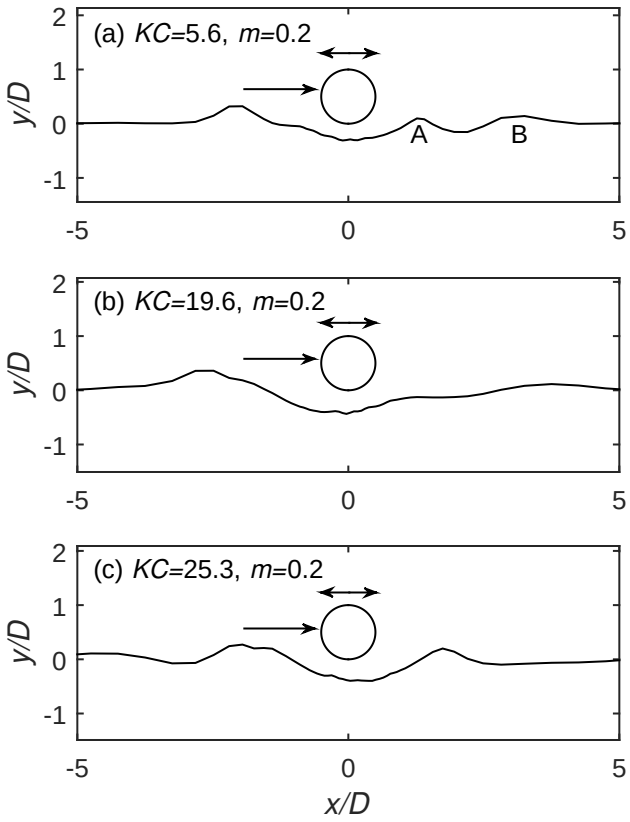

FIG. 10. Equilibrium scour profile of $KC = 5.6$**,** $m = 0.2$ **,** $KC = 19.6$**,** $m = 0.2$ **and** $KC = 25.3$**,** $m = 0.2$**.**

acterised by general profile symmetry in the vicinity of the pipeline, though some asymmetry develops further away, primarily in the form of one shoulder being larger than the other. In the pure-wave cases, as well as those with $m = 0.1$, our results suggest that the larger shoulder can emerge on either side of the pipeline. Alternatively, cases with $0.2 \leq m \leq 0.3$ primarily have a larger upstream shoulder, since emerging downstream shoulders tend to migrate downstream before slowly eroding as they become more exposed. This process can occur repeatedly as part of the dynamic equilibrium alluded to previously. A snapshot of this process can be seen in Figure 10a, where a new shoulder has just emerged (marked A), while the remnant of the previously developed shoulder (marked B) can still be seen migrating further downstream. In Figure 10b the downstream shoulder has been completely washed away and a new one is about to form, whereas in Figure 10c the downstream shoulder is close to maximum size and is just beginning to migrate downstream. For intermediate values of

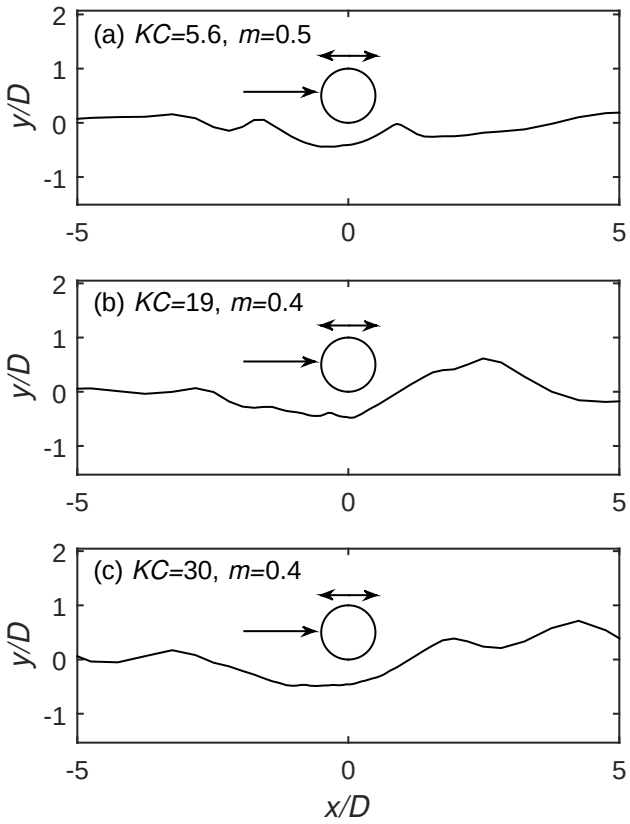

FIG. 11. Equilibrium scour profile of $KC = 5.6$**,** $m = 0.5$ **,** $KC = 19.6$**,** $m = 0.4$ **and** $KC = 30$**,** $m = 0.4$**.**

m and $KC \leq 30$ the present model results suggest that the scour profile can differ markedly from those typical of either pure-wave or pure-current conditions. Such profiles are characterized by a downstream shoulder much closer to the pipeline than the upstream shoulder. Typical examples are illustrated in Figure 11, where profiles for three different values of KC with intermediate values of m are shown. Given the relative strength of the current in these cases, these profiles can be considered as somewhat counter-intuitive, as the mean flow might have been expected to drive the downstream shoulder away from the pipeline. The sequence leading to the emergence of such profiles can be described as follows: During early stages of the scour process, a small shoulder develops downstream of the pipeline. With time this shoulder continues to grow, eventually causing flow separation on the lee side. This creates a lee-side vortex, which in turn causes additional growth, and eventual stability, of the shoulder. The flow patterns just described are illustrated in Figure 12, where the instantaneous

velocity field is plotted for the case with $KC = 5.6$ and $m = 0.5$ at $t/T_w = 0.3$. In these

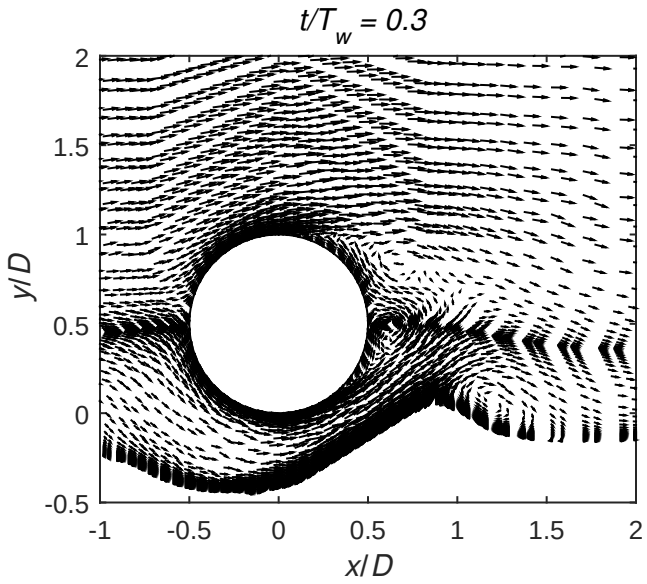

FIG. 12. Instantaneous velocity fields in the case of KC=5.6, m=0.5.

cases, the vortices shed from the bottom of the pipeline are relatively weak, hence limiting the lee-wake erosion. As experimental confirmation for this type of profile, one observed by Sumer and Fredsøe (1996) with $KC = 10$ and $m = 0.48$ is shown in Figure 13. Here it can be seen that the observed experimental profile shape is indeed very similar to that from the model having similar parameters i.e. $KC = 5.6$, $m = 0.5$, depicted in Figure 11a for example.

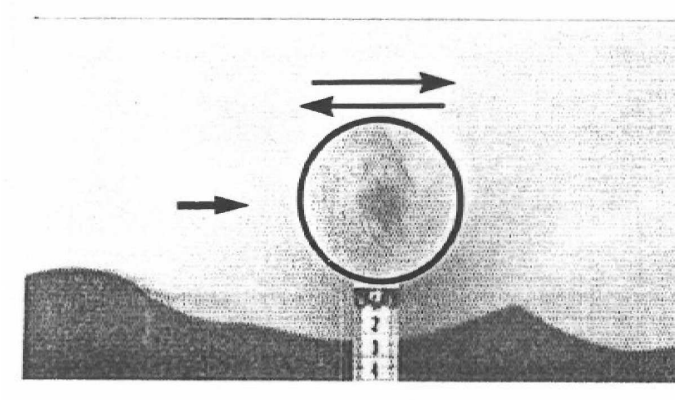

FIG. 13. Equilibrium scour profile of $KC = 10$, $m = 0.48$ (reprinted with permission from Sumer and Fredsøe, 1996).

Time scale

The time scale of scour qualitatively represents the time required for significant scour to develop. Being a fundamental quantity necessary for predicting the time sequence of scour beneath pipelines, this quantity is of significant engineering importance e.g. in the fatigue life assessment of submarine pipelines. While practical methods exist (see *e.g.* Fredsøe et al., 1992; Sumer and Fredsøe, 2002, p. 72) for predicting the scour time scale in both pure-current, as well as pure-wave conditions, this quantity has not previously been investigated and properly parametrized for generalized wave-plus-current flow environments, to the authors' knowledge. This knowledge gap will be filled by analysing the full matrix of numerical results in the present section.

In what follows, the scour time scales for all simulated cases have been determined by integration of the scour curves. Since an initial scour hole was prescribed, the time used for the integration then corresponds to the shifted time $t'^* = t^* + t^*_{shift}$, with the dimensionless time scale then calculated according to

$$T^* = \frac{\sqrt{g(s-1)d^3}}{D^2} T = \int_0^{t'^*_{max}} \frac{S_{max} - S}{S_{max}} dt'^*, \tag{17}$$

as suggested by Fuhrman et al. (2014), in which T is the dimensional time scale. An example for both the backward extrapolation of the scour curve, as well as the integrated quantity with respect to time, are shown in Figures 14a,b. As seen there, the time shift necessary due to the initial scour profile used in the simulations, does not typically make a major contribution to the time scale.

As a first attempt at parametrization of the wave-plus-current scour time scale, Figure 15 shows the computed non-dimensional time scales as a function of θ_{cw} for all cases considered in the present work. As a reference, the experimentally-based relation for the time scale of Fredsøe et al. (1992)

$$T^* = \frac{1}{50} \theta^{-\frac{5}{3}} \tag{18}$$

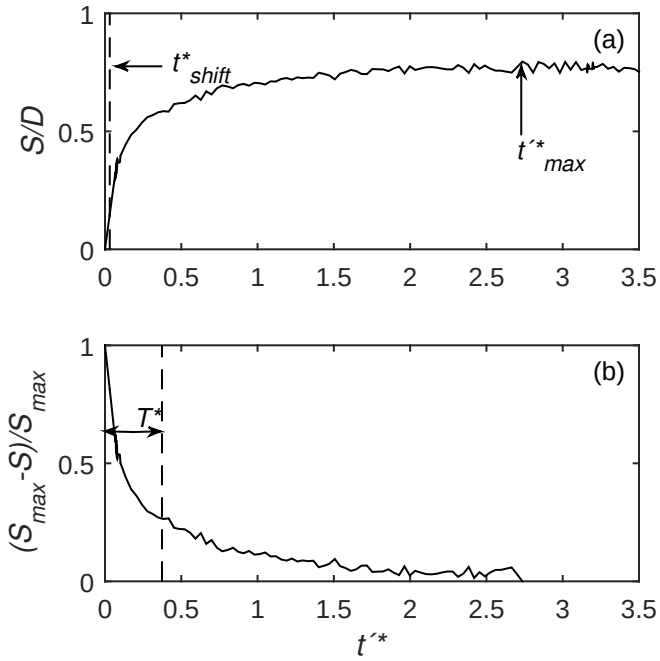

FIG. 14. Example of the calculation of the scour time scale T^* for $KC = 19.6$ with $m = 0.6$.

is also shown as the full line, which was demonstrated to be valid for both pure-current, as well as pure-wave, scour conditions. From Figure 15 it is seen that both the pure-current (diamonds, $m = 1$) and especially the pure-wave (circles, $m = 0$) results match the reference line (18) reasonably, generally consistent with the experimental findings of Fredsøe et al. (1992). Alternatively, the combined wave-plus-current results (asterisks, $0 < m < 1$) consistently lie either very close to or above the full line (18), implying a generally increased time scale for a given maximum Shields parameter, relative to either the pure-current or pure-wave limit.

Such an increase in the time scale (i.e. reduced scour rates) under combined wave-plus-current conditions should in fact be expected on physical grounds. A simple explanation follows: When m is higher than approximately 0.5 the free stream flow becomes unidirectional, oscillating between a strong and a weak current. In this way, it is effectively working like a strong current that is being periodically increased and decreased. This results in significant sediment transport, and hence scour, during the first half-period and much less during the

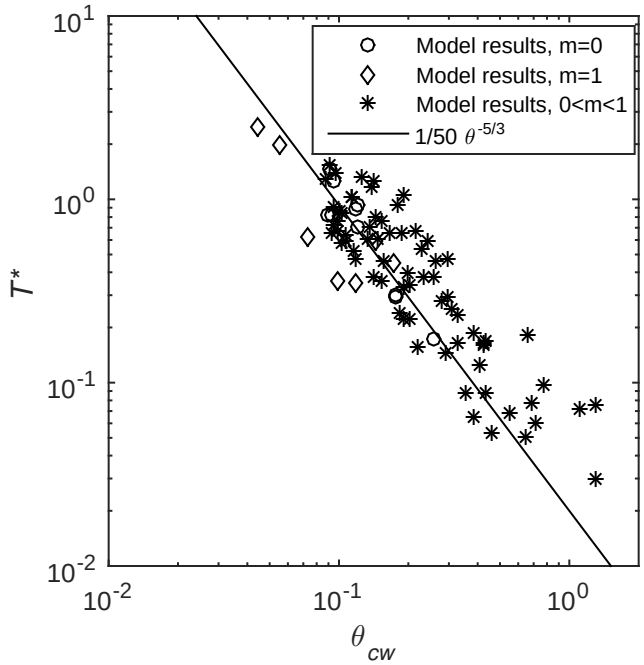

FIG. 15. Time scale of the scour development in the combined waves and current case.

second half-period. This behaviour is quantitatively illustrated in Figure 16, where the free stream velocity and scour time series over the first two periods for the case with $KC = 15$ and $m = 0.6$ are shown. The resulting "pump effect" can clearly be seen directly in the velocity time series (Figure 16a), as well as indirectly via the step-wise increase in the scour depth (Figure 16b) i.e. increasing scour when the flow is near maximum, followed by virtually no scour when the flow is near minimum. From the above description, it must be expected that the scour in a pure-current case having the same maximum Shields parameter will develop faster than in a combined wave-plus-current case, where the flow is near maximum for only a fraction of the overall time. Note that similar arguments might also be made for the pure-wave scour situations. However, in such cases significant sediment is being transported in both directions i.e. twice per wave period. Moreover, the largely symmetric profile shape in wave-dominated flows are also quite different than for cases involving current-dominated flows i.e. those involving high values of m, as established previously. From the above, it is now clear that the time scale T^* must depend not only on the Shields parameter θ_{cw}, but also on m, for generalized wave-plus-current situations. The Shields parameter θ_{cw} is obviously

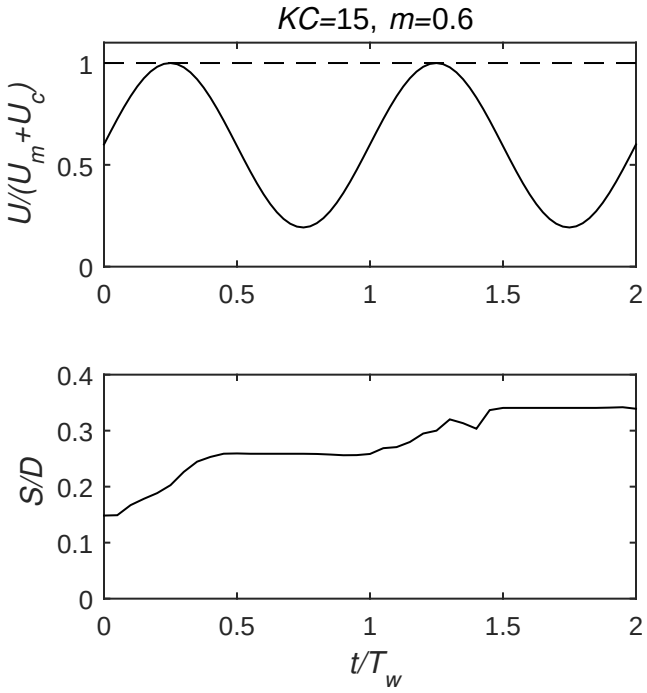

FIG. 16. Scour time and free stream velocity time series of $KC = 15$ with $m = 0.6$. The dashed line indicate the steady current situation having the same maximum velocity as the combined case.

important, as it will govern the maximum sediment transport, and hence scour, rates. Given that the non-dimensional time scale at both pure-wave and current limits scales as $\theta^{-5/3}$, see again (18), similar scaling should be expected in combined wave-current cases, as will be confirmed. Additionally, m-dependence must also be included to account for the the flow and scour rates being near maximum for only a limited fraction of the time. It can likewise be surmised that the time scale should not depend on KC, given that it depends only on θ even in the pure wave cases, see again (18). Following those arguments the time scale of the combined wave-plus-current cases will now be generalized to

$$T^* = \Gamma(m)\theta_{cw}^{-\frac{5}{3}}, \tag{19}$$

for predicting the scour time scale in combined wave-plus-current flows, where $\Gamma(m)$ is a (as yet, undetermined) function of m.

To begin determining $\Gamma(m)$, the computed dimensionless time scales T^* from Figure 15 are plotted against θ_{cw} in Figure 17, with results for various KC now grouped separately according to each of the discrete m considered. On each sub-figure the target (19) is also plotted (full lines), utilizing a constant value for $\Gamma(m)$ selected to best fit the individual data sets for each m. The only exceptions are those with $m = 0$ and $m = 1$, corresponding respectively to pure-wave and pure-current cases, where $\Gamma(m) = 1/50$ is utilized for consistency with (18). This also yields reasonable fits, as shown here and previously. It can be

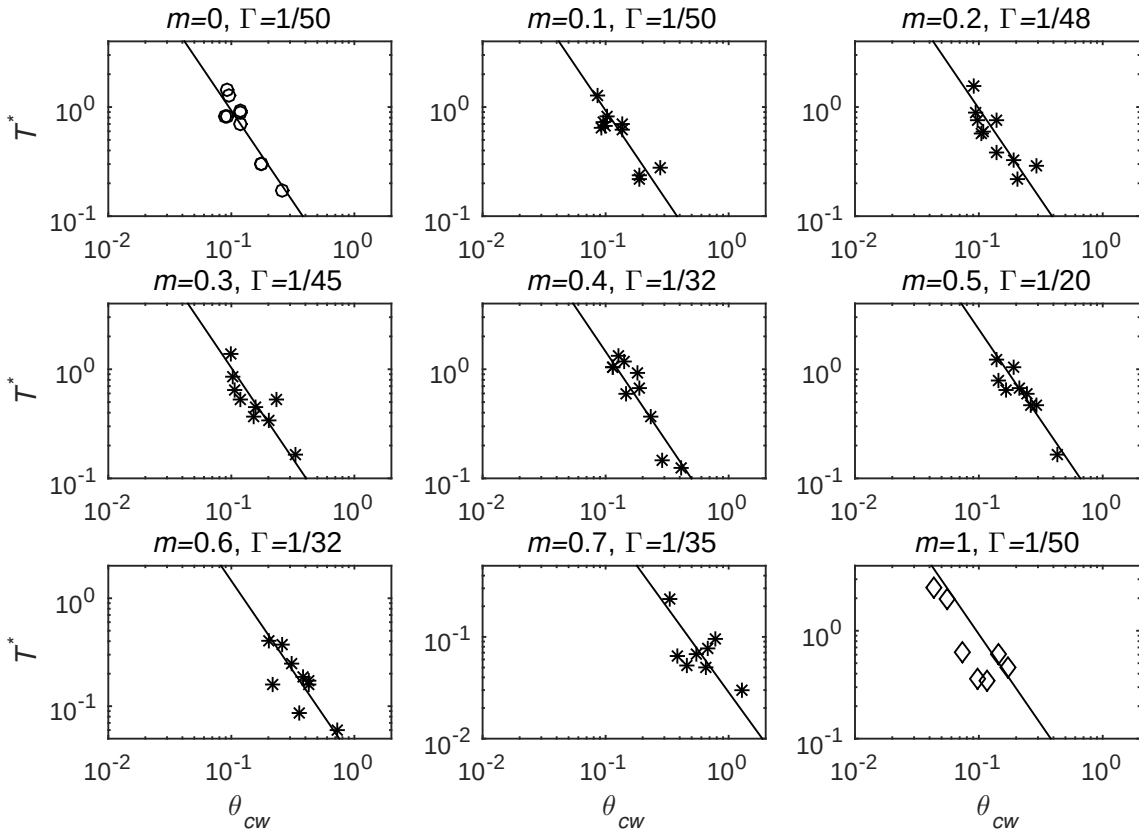

FIG. 17. Fit of the modelled time scales and equation (19)**.**

seen that (19), with properly selected $\Gamma(m)$ values, gives a quite good approximation for all cases i.e. spanning the full range of m. While there is inevitably some scatter in the results, this appears to be of the same order of magnitude as typically seen in experiments, see e.g. Fredsøe et al. (1992).

Inspired by the above, we will now seek a closed-form expression for the function $\Gamma(m)$.

The best-fit values for $\Gamma(m)$ for each discrete m from Figure 17, are now plotted as asterisks on Figure 18. Also shown as the full line is the function

$$\Gamma(m) = \frac{1}{50} + 0.015\left(e^{-350(m-0.5)^2} + e^{-25(m-0.53)^2}\right), \tag{20}$$

which matches the discrete values very well, while also tending naturally to the experimentally-based $\Gamma(m) = 1/50 = 0.02$ at both the $m = 0$ and $m = 1$ limits, again consistent with (18). From Figure 18 it is seen that $\Gamma(m)$ increases with m over the range $0 \leq m \leq 0.5$, meaning

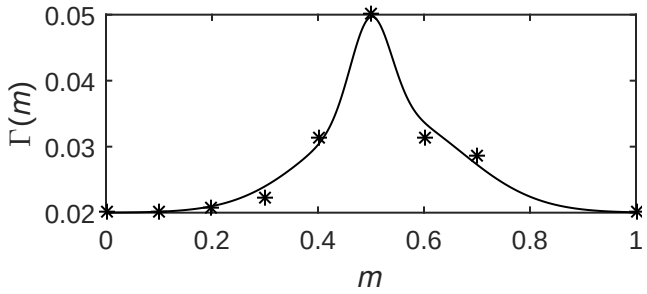

FIG. 18. Fit between (line) the suggested function for $\Gamma(m)$, (20) and (asterisk) the estimated values for $\Gamma(m)$.

that the scour time scale is larger than in pure-wave or pure-current cases. The function $\Gamma(m)$ then peaks at $m = 0.5$, before decreasing back to the steady-current value at $m = 1$. All of these results are generally consistent with the physical considerations discussed previously.

As a final check of the results, the computed time scale results from Figure 15 are re-cast in Figure 19, now in a form consistent with (19) i.e. as $T^*/\Gamma(m)$ versus θ_{cw}, while invoking (20). It is now seen that the considerable scatter previously evident in Figure 15 for the combined wave-plus-current results, is now significantly reduced. The tight clustering around the full line in Figure 19 hence confirms that the generalized expression (19) combined with (20) effectively unites the simulated time scales for pure-current, pure-wave, as well as the combined wave-plus-current flows. Based on the full consistency with the existing experimentally-based expression (18), the large matrix of physical conditions considered, as well as the good agreement between model and measured scour processes presented here, (19)

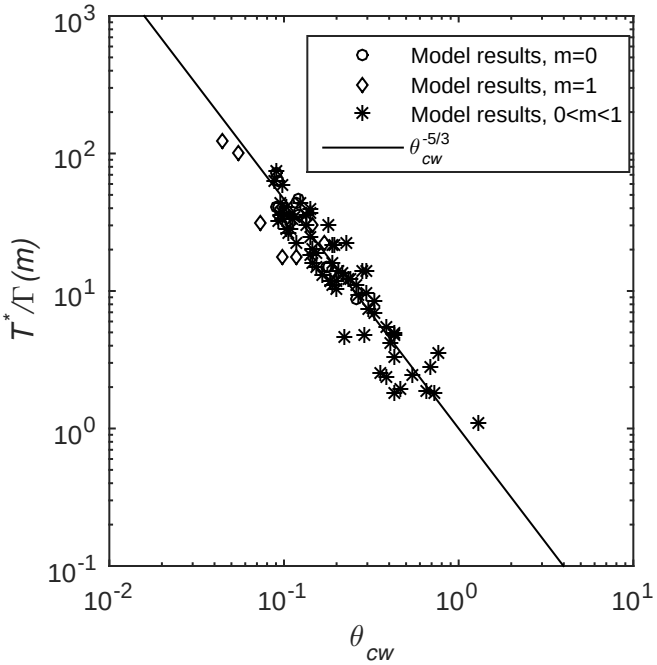

FIG. 19. Time scale in the combined wave-current flow as a function of the Shields parameter.

is believed to be appropriate for the engineering prediction of the scour time scale beneath pipelines for general wave-plus-current flows.

EXAMPLE CALCULATIONS

An example of how to calculate both the time scale of the scour development and the equilibrium scour depth in combined wave and current climates will now be given. Consider a situation with a $D = 30$ cm pipeline laid on the seabed exposed to waves with a period of T_w=10 s, a wave height $H = 2$ m, a water depth of $h = 10$ m and a mean current of $V = 0.6$ m/s. The grain size is $d = 0.5$ mm with a relative density $s = 2.65$. Note that these combine the conditions of the pure-wave and pure-current examples in (Sumer and Fredsøe, 2002, p. 46–48, 72–75).

Time scale

1. Calculate U_m utilizing linear wave theory by first calculating the wave number k by solving the linear dispersion relation

$$\left(\frac{2\pi}{T_w}\right)^2 = gk\tanh(kh) => k = 0.068 \text{ m}^{-1},$$

and then inserting into

$$U_m = \frac{\pi H}{T_w}\frac{\cosh(kz)}{\sinh(kh)} = 0.86 \text{ m/s},$$

where $z = 0$ is the distance from the bottom.

2. Estimate the maximum friction velocity of the wave U_{fw} by inserting into (9), by first finding the friction factor f_w according to $f_w = \max[f_w^{lam}, f_w^{smooth}, f_w^{rough}]$, where $f_w^{lam} = 0.0019$ is found from (10), $f_w^{smooth} = 0.0037$ is calculated from (11) and $f_w^{rough} = 0.0074$ is calculated from (12). Taking $f_w = f_w^{rough}$ yields $U_{fw} = 0.052$ m/s.
3. Calculate the friction velocity from the current alone by the flow resistance formula

$$U_{fc} = \frac{V\kappa}{\left(\ln\left(\frac{30h}{k_s}\right) - 1\right)} = 0.021 \text{ m/s},$$

where $\kappa = 0.4$ is the von Karman constant.

4. Estimate the velocity at the pipeline center U_c by assuming a rough logarithmic velocity profile

$$U_c = \frac{U_{fc}}{\kappa}\left(\ln\left(\frac{30\frac{D}{2}}{k_s}\right)\right) = 0.43 \text{ m/s}.$$

Inserting this into (6) then yields the non-dimensional parameter $m = 0.34$.

5. Calculate the Shields parameter of the wave $\theta_w = 0.34$ and the current $\theta_{cur} = 0.055$ by inserting U_{fw} and U_{fc} in (2). Insert these into (8) to calculate $\theta_m = 0.095$.
6. Calculate the characteristic undisturbed Shields parameter θ_{cw} from (7). This gives $\theta_{cw} = 0.43$.
7. Insert m into (20) to get $\Gamma = 0.026$ and insert this as well as θ_{cw} into (19) to get $T^* = 0.10$.

8. Finally, calculate the actual time scale from (17), giving $T = 210$ s ≈ 3.5 min.

For comparison it can be added that repeating the calculations with the naive approach i.e. inserting θ_{cw} into (18) yields $T = 162$ s ≈ 2.7 min which is somewhat faster.

Scour depth

1. From (5) calculate $KC = 28.5$.
2. Calculate $a_m = 0.55$ from (15) and $b_m = -1.12$ from (16). From (14) we now find $F = 0.80$.
3. Insert F as well as (4) into (13) to get $S_e/D = 0.48 \pm 0.16$ or $S_e = 0.14$ m $\pm\, 0.05$ m.

CONCLUSIONS

In this work results from a fully-coupled hydrodynamic and morphodynamic computational fluid dynamics (CFD) model for simulating wave-plus-current induced scour beneath submarine pipelines have been presented. The hydrodynamic model solves the incompressible Reynolds-averaged Navier Stokes (RANS) equations, coupled with k-ω turbulence closure. The model includes both bed and suspended load sediment transport descriptions, which drive seabed morphology based on the sediment continuity equation. A sand slide model is likewise incorporated, thus ensuring that the angle of repose is not exceeded on the seabed.

The model has been validated through comparison against experimental results of Mao (1986), who investigated scour beneath pipelines in steady current flows. The model has demonstrated the ability to accurately reproduce the profile shape evolution during the scour process in both clear-water and live-bed scour regimes. The model has likewise demonstrated the ability to yield equilibrium scour depths in good agreement with those observed by Mao (1986), over a wide range of Shields parameters. The present validation results for the scour induced by steady current-induced flows are complemented by those recently presented by Fuhrman et al. (2014) involving wave-induced scour processes.

The validated model has been subsequently utilized for the simulation of wave-plus-current induced scour involving 10 wave environments (characterized by KC numbers rang-

ing from $KC = 5.6$ to $KC = 51$) in combination with up to eight current environments (characterized by a current-strength parameter m ranging from $m = 0$ to $m = 0.7$, where $m = 0$ and $m = 1$, respectively, correspond to the pure-wave and pure-current limits). The model successfully predicts equilibrium scour depths and trends in general accordance with the experimentally-based empirical expressions for combined wave-current flows developed by Sumer and Fredsøe (1996) over the full range considered, serving as further validation.

The model results suggest that in wave-dominated flows (low m) the emerging scour profiles expectedly resemble those induced by pure-wave environments, whereas those emerging in current-dominated flows (medium to large m, depending somewhat on KC) resemble closely those induced by pure-current environments. Additionally, the model results suggest that situations having intermediate m i.e. situations that are neither wave- nor current-dominated, can result in equilibrium profiles characterized by a downstream shoulder closer to the pipeline than the upstream shoulder. This profile type has been reconciled directly with experimental observations of Sumer and Fredsøe (1996).

The matrix of simulated scour cases has been utilized to systematically investigate the scour time scale within combined wave-current flows. For a given maximum Shields parameter, it is found that the dimensionless scour time scale for wave-plus-current environments is larger than for pure-current situations. This has been explained on the following, simple, physical ground that in combined wave-current flows the Shields parameter is near maximum for only a fraction of the total time. Systematic assessment of the scour time series, grouped by discrete values of m, has resulted in a new and generalized analytical expression for the combined wave-plus-current dimensionless time scale. This is of the form $T^* = \Gamma(m)\theta_{cw}^{-\frac{5}{3}}$, where the function $\Gamma(m)$ is given in closed form within the paper. Importantly, this function tends to $\Gamma(m) = 1/50$ for both pure-wave and pure-current flows, hence unifying existing experimentally-based expressions for the time scale at these limits (Fredsøe et al., 1992). The resulting expression has been shown to match well the full range of simulated time scales considered. Given the demonstrated collective accuracy of the model in simulating scour

processes due to currents, waves (Fuhrman et al., 2014), as well as their combination, it is believed that the proposed expression for the generalized wave-plus-current scour time scale is appropriate for engineering use.

ACKNOWLEDGEMENTS

The authors acknowledge support from the European Union project ASTARTE–Assessment, Strategy And Risk Reduction for Tsunamis in Europe, Grant no. 603839 (FP7-ENV-2013.6.4-3). The third author additionally acknowledges Innovative Multi-purpose Offshore Platforms: Planning, Design and Operation (MERMAID), 20122016, Grant Agreement No. 288710 of European Commission, 7th Framework Programme for Research.

REFERENCES

Baykal, C., Sumer, B. M., Fuhrman, D. R., Jacobsen, N. G., and Fredsøe, J. (2015). "Numerical investigation of flow and scour around a vertical circular cylinder." *Phil. Trans. Roy. Soc. A*, 373, 1–21.

Bernetti, R., Bruschi, R., Valentini, V., and Ventur, M. (1990). "Pipelines placed on erodible seabeds." *Proc 9th International Conference on Offshore Mechanics and Arctic Engineering*, Vol. 5, Houston, Texas, 155–164.

Brørs, B. (1999). "Numerical modeling of flow and scour at pipelines." *J. Hydraul. Eng. ASCE*, 125, 511–523.

Cebeci, T. and Chang, K. C. (1978). "Calculation of incompressible rough-wall boundary-layer flows." *AIAA J.*, 16(7), 730–735.

Cheng, L., Yeow, K., Zang, Z., and Li, F. (2014). "3D scour below pipelines under waves and combined waves and currents." *Coast. Eng.*, 83, 137–149.

Engelund, F. and Fredsøe, J. (1976). "A sediment transport model for straight alluvial channels." *Nordic Hydrology*, 7(5), 293–306.

Fredsøe, J., Andersen, K. H., and Sumer, B. M. (1999). "Wave plus current over a ripple-covered bed." *Coast. Eng.*, 38(4), 177–221.

Fredsøe, J. and Deigaard, R. (1992). *Mechanics of Coastal Sediment Transport.* World Scientific, Singapore.

Fredsøe, J., Sumer, B. M., and Arnskov, M. M. (1992). "Time scale for wave/current scour below pipelines." *Int. J. Offshore Polar Eng.*, 2(1), 13–17.

Fuhrman, D. R., Baykal, C., Sumer, B. M., Jacobsen, N. G., and Fredsoe, J. (2014). "Numerical simulation of wave-induced scour and backfilling processes beneath submarine pipelines." *Coast. Eng.*, 94, 10–22.

Fuhrman, D. R., Schløer, S., and Sterner, J. (2013). "RANS-based simulation of turbulent wave boundary layer and sheet-flow sediment transport processes." *Coast. Eng.*, 73, 151–166.

Hansen, E. A. (1992). "Scour below pipelines and cables: A simple model." *Proc. 11th Offsjore Mechanics and Arctic Engineering Conference*, Vol. V, ASME, 133–138.

Hoffmans, G. J. C. M. and Verheij, H. J. (1997). *Scour Manual.* A.A.Balkema, Rotterdam.

Jacobsen, N. G., Fredsøe, J., and Jensen, J. H. (2014). "Formation and development of a breaker bar under regular waves. Part 1: Model description and hydrodynamics." *Coast. Eng.*, 88, 182–193.

Jacobsen, N. G., Fuhrman, D. R., and Fredsøe, J. (2012). "A wave generation toolbox for the open-source CFD library: OpenFoam (R)." *Int. J. Numer. Meth. Fluids*, 70(9), 1073–1088.

Kazeminezhad, M. H., Yeganeh-Bakhtiary, A., Etemad-Shahidi, A., and Baas, J. H. (2012). "Two-phase simulation of wave-induced tunnel scour beneath marine pipelines." *J. Hydraul. Eng. ASCE*, 138(6), 517–529.

Liang, D. and Cheng, L. (2005a). "Numerical model for wave-induced scour below a submarine pipeline." *J. Waterw. Port C-ASCE*, 131, 193–202.

Liang, D. and Cheng, L. (2005b). "Numerical modeling of flow and scour below a pipeline in currents Part I. Flow simulation." *Coast. Eng.*, 52(1), 25–42.

Liang, D., Cheng, L., and Li, F. (2005). "Numerical modeling of flow and scour below a pipeline in currents - Part II. Scour simulation." *Coast. Eng.*, 52(1), 43–62.

Lucassen, R. J. (1984). "Scour underneath submarine pipelines. Report No. PL-4 2A, Netherlands Marine Tech. Res., Netherlands Industrial Council for Oceanology, Delft University of Technology, Delft, The Netherlands.

Mao, Y. (1986). *The interaction between a pipeline and an erodible bed.* Inst. of Hydrodynamic and Hydr. Engng., Technical University of Denmark, Series Paper No. 39, March, 169 p.

Myrhaug, D., Ong, M. C., Føien, H., Gjengedal, C., and Leira, B. J. (2009). "Scour below pipelines and around vertical piles due to second-order random waves plus current." *Ocean Eng.*, 36(2), 605–616.

Roulund, A., Sumer, B. M., Fredsøe, J., and Michelsen, J. (2005). "Numerical and experimental investigation of flow and scour around a circular pile." *J. Fluid Mech.*, 534, 351–401.

Soulsby, R. L. (1995). "Bed shear-stresses due to combined waves and currents." *Advances in coastal morphodynamics*, M. J. F. Stive, H. D. Vriend, J. Fredsøe, L. Hamm, R. L. Soulsby, C. Teisson, and J. C. Winterwerp, eds., Delft Hydraulics, Delft, NL, 4–20 to 4–23.

Sumer, B. M. and Fredsøe, J. (1990). "Scour below pipelines in waves." *J. Waterw. Port C-ASCE*, 116(3), 307–323.

Sumer, B. M. and Fredsøe, J. (1996). "Scour around pipelines in combined waves and current." *Proceedings of the International Conference on Offshore Mechanics and Arctic Engineering - OMAE*, G. Rosa, ed., Vol. 5, ASME, 595–602.

Sumer, B. M. and Fredsøe, J. (2002). *The Mechanics of Scour in the Marine Environment*. World Scientific, Singapore.

Whitehouse, R. (1998). *Scour at Marine Structures: A Manual for Practical Applications*. Thomas Telford Ltd., London.

Wilcox, D. C. (2006). *Turbulence Modeling for CFD*. DCW Industries, Inc., La Canada, California, 3rd edition.

Wilcox, D. C. (2008). "Formulation of the k-ω turbulence model revisited." *AIAA J.*, 46(11), 2823–2838.

Zanganeh, M., Yeganeh-Bakhtiary, A., and Wahab, A. K. A. (2012). "Lagrangian coupling two-phase flow model to simulate current-induced scour beneath marine pipelines." *Applied Ocean Research*, 38, 64–73.

Zhao, Z. and Fernando, H. J. S. (2007). "Numerical simulation of scour around pipelines using an euler-euler coupled two-phase model." *Environmental Fluid Mechanics*, 7(2), 121–142.